nature structural & molecular biology

ARTICLES

https://doi.org/10.1038/s41594-018-0114-9

The ZZ domain of p300 mediates specificity of the adjacent HAT domain for histone H3

Yi Zhang[1,6], Yongming Xue[2,3,6], Jiejun Shi[4], JaeWoo Ahn[1], Wenyi Mi[2,5], Muzaffar Ali[1], Xiaolu Wang[2,5], Brianna J. Klein[1], Hong Wen[2,5], Wei Li[4], Xiaobing Shi[2,3,5*] and Tatiana G. Kutateladze[1*]

Human p300 is a transcriptional co-activator and a major acetyltransferase that acetylates histones and other proteins facilitating gene transcription. The activity of p300 relies on the fine-tuned interactome that involves a dozen p300 domains and hundreds of binding partners and links p300 to a wide range of vital signaling events. Here, we report a novel function of the ZZ-type zinc finger (ZZ) of p300 as a reader of histone H3. We show that the ZZ domain and acetyllysine-recognizing bromodomain of p300 play critical roles in modulating p300 enzymatic activity and its association with chromatin. The acetyllysine binding function of bromodomain is essential for acetylation of histones H3 and H4, whereas interaction of the ZZ domain with H3 promotes selective acetylation of the histone H3K27 and H3K18 sites.

P300 is critical in cell growth, differentiation, apoptosis, and DNA repair and is closely linked to many human diseases, cancer in particular[1–3]. It functions as a scaffolding protein that recruits numerous nuclear components, including transcription factors, co-activators, and subunits of the RNA polymerase II complex to chromatin[4–6]. p300 possesses an intrinsic histone acetyltransferase (HAT) activity and acetylates histones, directly altering chromatin structure and promoting expression of specific genes[7–9]. This large, ~300 kDa, evolutionarily conserved enzyme is functionally related to and cooperates with paralogous CBP, and both share the same domain architecture consisting of a diverse set of protein- and DNA-binding modules. Along with the N-terminal nuclear receptor interaction domain, a transcriptional adaptor zinc-finger 1 (TAZ1), and a kinase-inducible CREB interaction region (KIX), p300 contains a combination of a bromodomain, a RING finger, and a plant homeodomain (PHD) finger preceding the catalytic HAT domain (Fig. 1a). The HAT domain is followed by a ZZ-type zinc finger, another TAZ domain (TAZ2), and an interferon-binding domain. Although these domains predominantly associate with activators, basal transcription factors, and components of the multi-subunit HAT complexes, some have also been implicated in control of the p300 catalytic activity[10,11]. The HAT domain itself is regulated through its autoinhibitory loop (AIL), which in a hypoacetylated form suppresses the catalytic activity but releases the inhibition on hyperautoacetylation[7,12]. An additional layer of p300 regulation has been suggested based on the recent structure of the p300 region encompassing bromodomain, RING, PHD, and the HAT domain (BRPH), in which the RING finger aids in the inhibition through occluding the HAT active site in conjunction with AIL[13]. Owing to their crucial role in a magnitude of signaling pathways, biological activities of p300 domains have been studied extensively; however, the function of the ZZ domain remains unclear. In this study, we show that the ZZ domain of p300 recognizes histone H3 tail and therefore represents a novel epigenetic reader. Our findings suggest that the histone binding function of ZZ and acetyllysine binding function of bromodomain are essential in chromatin targeting and catalytic activities of p300. Particularly, recognition of histone H3 by the ZZ domain promotes acetylation of primarily histone H3K27 and H3K18 sites.

Results

The ZZ domain of p300 targets histone H3. The histone binding activity of the ZZ domain of p300 (p300-ZZ) was originally identified by peptide pull-down experiments (Fig. 1b,c). We found that glutathione *S*-transferase (GST)-tagged p300-ZZ binds to the residues 1–22 of the histone H3 tail but does not recognize other regions of H3 or other histones, and that common single post-translational modifications (PTMs) on H3 do not affect this interaction (Fig. 1b,c). To characterize the binding in detail, we expressed p300-ZZ as an ^{15}N-labeled protein and tested it in ^{1}H,^{15}N heteronuclear single quantum coherence (^{1}H,^{15}N HSQC) experiments (Fig. 1d). Gradual addition of the $H3_{1-12}$ peptide (residues 1–12 of H3) to the p300-ZZ NMR sample led to large resonance changes. These changes were in the intermediate exchange regime on the NMR timescale and suggested a tight binding. In agreement, an 8.8-μM binding affinity of p300-ZZ for the $H3_{1-12}$ peptide was measured by fluorescence assays (Fig. 1e,f). Methylation of H3K4, a common target of epigenetic readers, or acetylation of H3K4 had no effect, as almost identical patterns of resonance changes were observed in NMR titration experiments, and the comparable binding affinities were measured for the correspondingly modified peptides (Fig. 1e and Supplementary Figs. 1a and 2). Importantly, the K_d value for the p300-ZZ/$H3_{1-12}$ interaction was in the range of binding affinities exhibited by the majority of histone binding modules[14–16], corroborating the notion that the ZZ domain of p300 is a new member of the family of epigenetic readers that select for histone H3.

[1]Department of Pharmacology, University of Colorado School of Medicine, Aurora, CO, USA. [2]Department of Epigenetics and Molecular Carcinogenesis, Center for Cancer Epigenetics, The University of Texas MD Anderson Cancer Center, Houston, TX, USA. [3]Genetics and Epigenetics Graduate Program, The University of Texas MD Anderson Cancer Center UTHealth Graduate School of Biomedical Sciences, Houston, TX, USA. [4]Dan L. Duncan Cancer Center, Department of Molecular and Cellular Biology, Baylor College of Medicine, Houston, TX, USA. [5]Center for Epigenetics, Van Andel Research Institute, Grand Rapids, MI, USA. [6]These authors contributed equally: Y. Zhang, Y. Xue. *e-mail: Xiaobing.Shi@vai.org; tatiana.kutateladze@ucdenver.edu

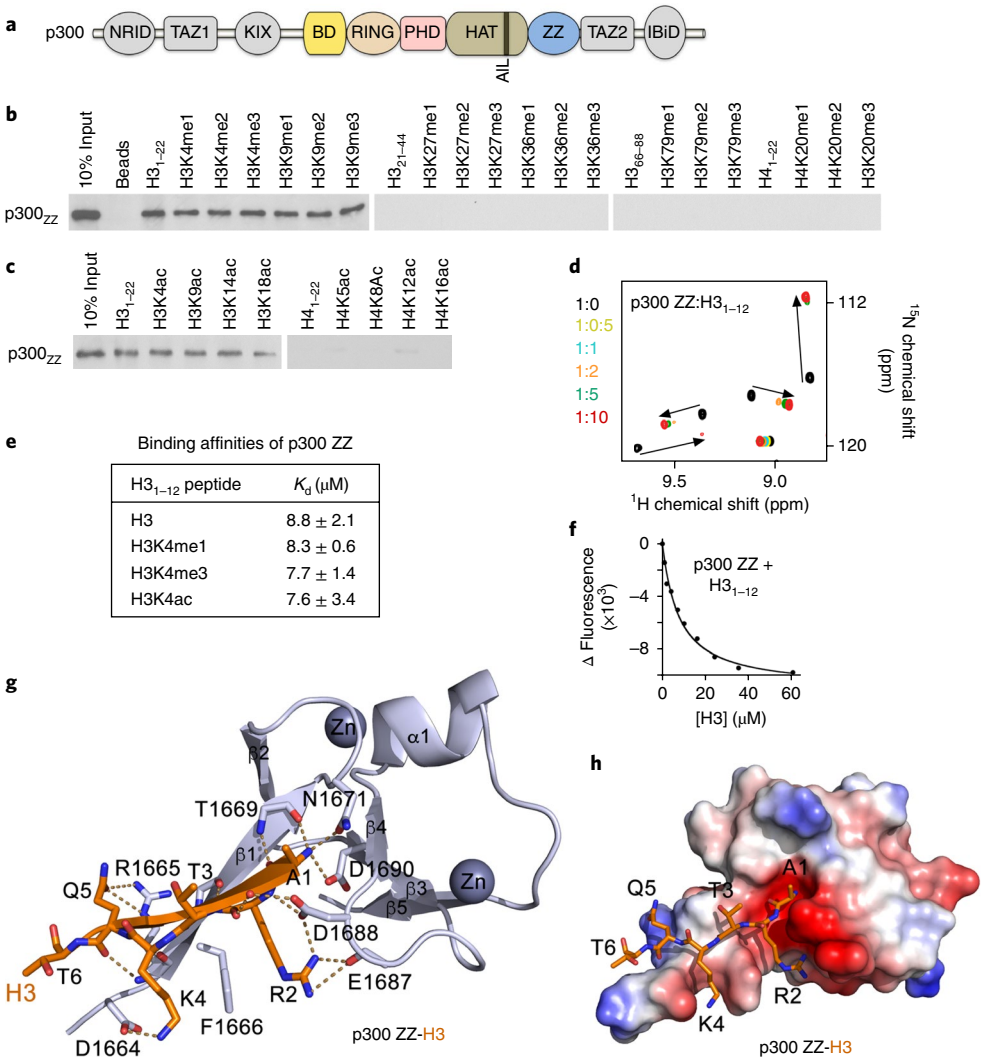

Fig. 1 | The ZZ domain of p300 recognizes histone H3. a, Schematic representation of p300 domain architecture. **b**,**c**, Peptide pull-down assays of the p300 ZZ domain with the indicated histone peptides. Uncropped blot images are shown in Supplementary Data Set 1. **d**, Superimposed ^{1}H,^{15}N HSQC spectra of p300-ZZ collected upon titration with H3 peptide (residues 1–12 of H3). Spectra are color coded according to the protein-to-peptide molar ratio. **e**, Binding affinities of wild-type p300-ZZ for the indicated histone peptides measured by tryptophan fluorescence. The experiments were carried out in triplicate for H3 and H3K4ac and in duplicate for methylated H3. **f**, Representative binding curve used to determine the K_d values by fluorescence. See also Supplementary Fig. 2. **g**, A ribbon diagram of the p300-ZZ domain (light blue) in complex with histone H3 tail (residues 1–6) (orange). **h**, Electrostatic surface potential of p300-ZZ is colored blue (positive charge) and red (negative charge) with the bound histone H3 tail shown in stick representation. BD, bromodomain; IBiD, interferon-binding domain.

Molecular mechanism of the p300-ZZ association with H3. To elucidate the molecular basis for the recognition of the H3 tail, we determined a 2.0-Å-resolution crystal structure of the p300-ZZ/H3 complex using the chimeric construct containing residues 1–6 of H3 linked to the residues 1,663–1,713 of p300 (Fig. 1g,h). The ^{1}H,^{15}N HSQC spectra of the linked H3–ZZ construct and of the isolated ZZ domain in the presence of a tenfold excess of $H3_{1–12}$ peptide overlaid well, confirming that the linked and unlinked ZZ–H3 complexes adopt identical structures in solution (Supplementary Fig. 3). The structure showed two H3–ZZ molecules forming the complex in which the H3 region of one molecule is bound to the ZZ domain of another molecule (Table 1 and Supplementary Fig. 4a).

The p300-ZZ fold is stabilized by two zinc-binding clusters, a couple of twisted two- and three-stranded antiparallel β-sheets, and a short α-helix (Fig. 1g). The histone residues pair with the first β-strand (residues 1,665–1,669 of ZZ), creating the third antiparallel β-stand, and make extensive intermolecular contacts with the domain (Fig. 1g). Characteristic β-sheet interactions are observed between the backbone amides of Ala1, Thr3, and Gln5 of H3 and T1669, V1667, and R1665 of the ZZ domain. Ala1 occupies a highly negatively charged binding site where the NH_3^+ group of Ala1 is anchored through the hydrogen bonds with T1669 and N1671 and a salt bridge with D1690 (Figs. 1g,h and 2a). The guanidinium moiety of Arg2 is restrained via a salt bridge with the carboxyl group of D1688 and hydrogen bonds with the backbone carbonyl oxygen of E1687, whereas the backbone amide of Arg2 is involved in direct and water-mediated hydrogen bonding contacts with D1688. The side chain of Lys4 lays in a groove formed by the aromatic ring of F1666 and the side chain of D1664, the negatively charged carboxylic group of which forms a salt bridge with the ε-amino group of Lys4 (Figs. 1g and 2b). The formation of the salt bridge most likely accounts for the indifference of p300-ZZ towards PTMs on H3K4, which would augment cation-π and hydrophobic interactions with F1666 but diminish the electrostatic contact with D1664. The side

Table 1 | Data collection and refinement statistics for the ZZ/H3 complex

	H3/ZZ (PDB 6DS6)
Data collection	
Space group	$P43_12$
Cell dimensions	
a, *b*, *c* (Å)	44.0, 44.0, 85.9
α, β, γ (°)	90.0, 90.0, 90.0
Wavelength	1.278
Resolution (Å)[a]	39.18–1.95 (1.98–1.95)[a]
R_{merge}	7.7 (29.6)
$I/\sigma(I)$	71.4 (2.5)
Completeness (%)	99.2 (94.5)
Redundancy	22.3 (9.2)
Refinement	
Resolution (Å)	21.32–1.95
No. reflections	11,533
R_{work}/R_{free}	0.2070/0.2532
No. atoms	
Protein	465
Zinc	2
Chloride	1
Water	56
B factors	
Protein	44.9
Zinc	53.7
Chloride	65.7
Water	56.0
R.m.s. deviations	
Bond lengths (Å)	0.007
Bond angles (°)	0.922

[a]Values in parentheses refer to data in the highest resolution shell. Datasets collected from a single crystal.

chain of Gln5 is hydrogen bonded to the guanidinium group of R1665. This mechanism for the coordination of H3 is distinctly different and distinguishes the ZZ domain from all currently known readers, including those that bind to the N terminus of H3 (Supplementary Fig. 4b,c).

The critical role of the Ala1 recognition was substantiated by testing truncated variants of H3 and mutating the binding site residues in p300-ZZ (Fig. 2). Peptide pull-down and NMR experiments with various fragments of histone H3 confirmed that at least the first two residues of H3 are required for the interaction (Fig. 2c,d,h). The absence of chemical shift changes in $^{1}H,^{15}N$ HSQC spectra of p300-ZZ upon titration with either the AGSGSG peptide, Ac-RTKacQTARKSTG (H3K4ac$_{2-12}$), or Ac-H3$_{3-10}$ suggested that both the H3 sequence and the presence of the positive charge on Ala1 are necessary for the interaction (Fig. 2h). Replacement of Ala1 with a larger residue, valine, in H3A1V$_{1-6}$ resulted in a reduction in the binding ~threefold, and very small resonance perturbations in p300-ZZ upon addition of H4$_{1-9}$(Ser1) indicated an almost negligible binding. Substitution of the Ala1-binding site residues, N1671 or D1690, with an alanine abolished the interaction of p300-ZZ with H3 peptides or calf thymus histones in pull-down assays (Fig. 2e and Supplementary Fig. 5) and NMR titrations (Fig. 2c). Further, mutation of D1688 and F1666 or deletion of the first five (1,663–1,667) residues in p300-ZZ substantially reduced the binding, pointing to the essential role of the Arg2 and Lys4 coordination and formation of the β-sheet, respectively (Fig. 2e and Supplementary Figs. 1b and 5b).

Recruitment of p300 to chromatin depends on synergistic histone binding functions of ZZ and bromodomain. The importance of the histone binding activity of the ZZ domain for the association of p300 with chromatin was examined by chromatin immunoprecipitation (ChIP) followed by western blot and salt fractionation assays in H1299 cells stably expressing p300 fragment containing bromodomain-RING-PHD-HAT-ZZ-TAZ2 (BRPHZT) (Fig. 2f,g and Supplementary Fig. 5c–e). Bromodomain of p300/CBP was previously shown to target acetylated lysine residues in histone and non-histone proteins, and the bromodomain-RING-PHD (BRP) region binds hyperacetylated nucleosomes and acetyllysine-containing peptides[13,17–23]. In agreement, our NMR titration experiments confirmed that bromodomain within BRP associates with an acetylated peptide but does not recognize unmodified H3$_{1-19}$, which is the ligand of ZZ (Supplementary Fig. 6a). Deletion or loss-of-function mutations of either ZZ (ΔZZ, N1671A, and D1690A) or bromodomain (ΔBD and N1132A) substantially reduced the association of p300 BRPHZT with chromatin containing acetyllysine marks, and deletion or mutation of both domains had an additive effect (Fig. 2f,g and Supplementary Fig. 5c–e). These data indicate that both readers, bromodomain and ZZ, contribute to the interaction of p300 BRPHZT with chromatin although their ligands differ: ZZ binds to the N terminus of H3 independent of PTMs, whereas bromodomain binds to various histone sequences acetylated at lysine residues, favoring poly-acetylated H4[13,17,21]. The fact that the impaired histone binding activity of either ZZ or bromodomain led to such a notable decrease in chromatin binding of p300 BRPHZT suggests that the two interactions cooperate in the recruitment or retention of p300 at chromatin. Deletion of AIL appears to have no effect on the association of BRPHZT with chromatin (Fig. 2g and Supplementary Fig. 5d).

P300-ZZ and HAT cooperate in binding to H3 tail. Much like the BRP region preceding the HAT domain, the following ZZ domain is in close proximity to the HAT domain with only ~two residues connecting the domains. We found that the isolated ZZ and HAT domains interact only weakly, as the HAT domain caused very small changes in ZZ; however, subsequent titration of H3$_{1-12}$ peptide resulted in large resonance perturbations, suggesting that the histone binding function of ZZ is preserved in the presence or absence of HAT (Fig. 3a). Analysis of the fluorescence-derived binding curves for the interaction of the natively linked HAT-ZZ construct with H3$_{1-12}$ peptide required a two-site binding model, which implies that both HAT and ZZ are engaged with the peptide. The fitting yielded two K_d values of 2.6 μM and 29 μM, which are comparable to K_ds measured for the isolated ZZ and HAT domains (8.8 μM and 38 μM, respectively) (Fig. 3b, c). The longer H3 peptide (residues 1–31, H3$_{1-31}$), however, was bound by HAT-ZZ substantially tighter, revealing a cooperative binding and an *in cis* mechanism (Fig. 3b–d and Supplementary Fig. 2b). In support, the cooperativity was no longer observed for binding of the HAT-ZZ$_{N1671A}$ construct that harbors loss-of-function ZZ to the H3$_{1-31}$ peptide (Fig. 3b). The cooperative binding was also eliminated in wild-type HAT-ZZ when the histone H3$_{5-31}$ peptide, in which the ZZ-targeted sequence is deleted, was used as ligand. The binding affinities of wild-type HAT-ZZ and HAT-ZZ$_{N1671A}$ for the H3$_{5-31}$ peptide (K_d = 21 μM and 17 μM, respectively) were essentially the same as the binding affinity of the isolated HAT domain for H3$_{5-31}$ (K_d = 16 μM).

Interaction of p300-ZZ with H3 directs acetylation of H3K27 and H3K18 in vitro. The BRP region has been shown to associate

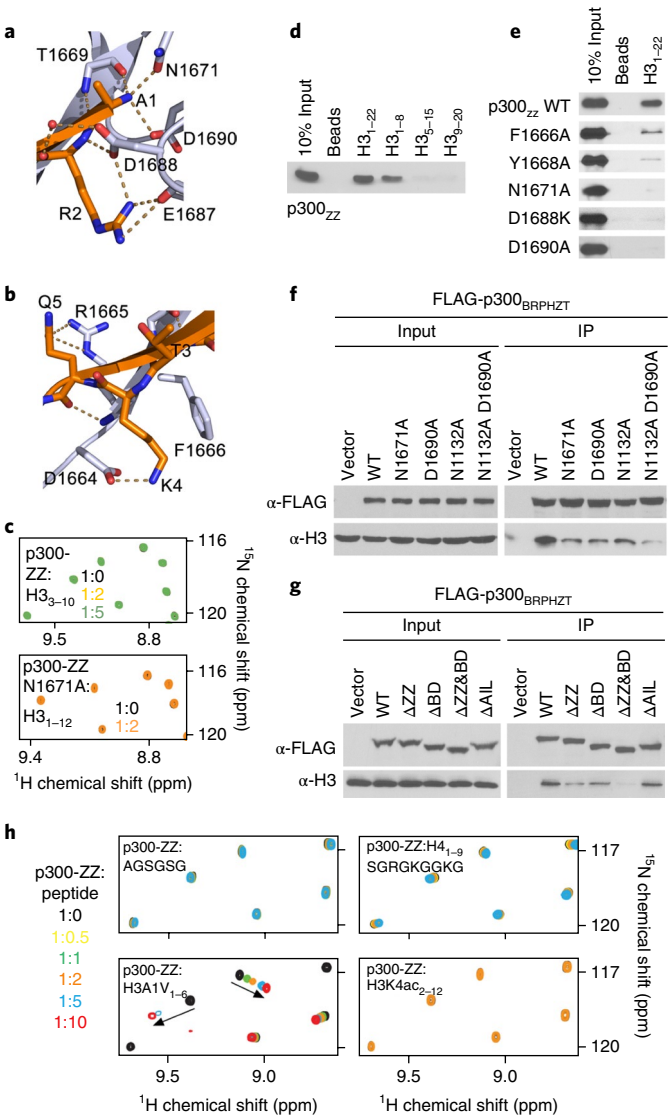

Fig. 2 | Molecular basis for the recognition of H3 tail by p300-ZZ. **a**, Zoom-in view of the histone H3 Ala1 binding site. **b**, Zoom-in view of the histone H3 Lys4 binding site. **c**, Superimposed ^{1}H,^{15}N HSQC spectra of p300-ZZ (wild type and N1671A mutant) collected upon titration with indicated H3 peptides. Spectra are color coded according to the protein-to-peptide molar ratio. **d**, Peptide pull-down assays for p300-ZZ using indicated histone H3 peptides. **e**, Peptide pull-down assays using wild-type and mutated p300-ZZ. **f**,**g**, Western blot analysis of ChIP of wild-type FLAG-p300$_{BRPHZT}$ and indicated point- and deletion-mutants in H1299 stable cells. **h**, Superimposed ^{1}H,^{15}N HSQC spectra of p300 ZZ collected upon titration with indicated peptides. Spectra are color coded according to the protein-to-peptide molar ratio shown on the left. Uncropped blot images of panels **d**–**g** are shown in Supplementary Data Set 1. WT, wild type.

with the HAT domain with the binding affinity of 1.6 μM[13]. We confirmed the direct and robust interaction through monitoring rapid disappearance of resonances of the ^{15}N-labeled BRP region induced by the unlabeled HAT domain in ^{1}H,^{15}N HSQC experiments (Supplementary Fig. 6). However, this interaction was weakened when the linked HAT-ZZ was titrated in, indicating a conformational mobility within the HAT-ZZ construct that may alter the priming of BRP (Supplementary Fig. 6b). The dynamic organization of the adjacent to the HAT domain modules may facilitate substrate and acyl-CoA association, enlarge the substrate pool of p300, and mediate its HAT activity. To determine whether the ZZ/H3 interaction affects the catalytic activity of p300, we carried out in vitro HAT assays using the p300-BRPHZ fragment and reconstituted unmodified nucleosomes. We found that wild-type p300-BRPHZ acetylates H3 on H3K27 and H3K18 robustly, but very little acetylation was detected on H3K9 and H3K4 (Fig. 3e–k and Supplementary Fig. 7a). Mutation of the ZZ residues critical for binding to H3, N1671 and D1690, to an alanine in p300-BRPHZ substantially reduced the HAT activity on H3K27 and H3K18 but did not affect acetylation on H3K4 and H3K9. Likewise, the deletion of ZZ led to a considerable reduction of acetylation on H3K27 and H3K18; however, it had no effect on acetylation of H3K4 and H3K9 (Fig. 4a–e). Furthermore, the HAT activity of p300-BRPHZ on the nucleosome, in which the first two residues of H3 (Ala1-Arg2, that are required for the binding of ZZ) were deleted, was severely compromised (Fig. 4f,g). In contrast, mutation of N1132 that impairs acetyllysine binding of bromodomain led to a substantial decrease in acetylation of all lysine residues tested, H3K4, K3K9, H3K18, and H3K27 (Fig. 3e–k). These results suggest that the acetyllysine binding function of bromodomain is necessary for the overall catalytic activity of p300-BRPHZ on the nucleosome, whereas the ability of p300-BRPHZ to acetylate primarily H3K27 and H3K18 is due to binding of the ZZ domain to H3.

p300 bromodomain was previously proposed to bind acetylated substrates to facilitate acetylation at other sites[13,19]. Although we used unmodified nucleosomes in the HAT assays, the initial acetylation of histones by p300-BRPHZ can provide a feed-forward mechanism, supporting this idea. Potentially, AIL of the HAT domain can also be a ligand for bromodomain (Fig. 4h), as this loop is autoacetylated in endogenous and recombinant p300[12], and bromodomain of CBP interacts with the AIL peptide acetylated at K1596[19]. Although binding affinities of wild-type p300-BRPHZ, p300-B$_{N1132A}$RPHZ, and p300-BRPH$_{\Delta AIL}$Z for H3$_{1–31}$ suggest that abrogating acetyllysine binding of bromodomain or deleting AIL has little effect on the association of p300-BRPHZ with this peptide (Fig. 5a,b), comparison of acetylation levels produced by wild-type p300-BRPHZ and p300-BRPH$_{\Delta AIL}$Z in 10 min reveals that the deletion of AIL stimulates the HAT activity of p300-BRPHZ (Fig. 4a–e). These data are in agreement with the previous reports on inhibition of the p300 catalytic activity by hypoacetylated AIL[12]. It was proposed that the hypoacetylated AIL might contact a negatively charged patch on the HAT domain surface blocking the active site, whereas acetylation of AIL releases this loop freeing the active site[7,12]. At least ten lysine residues in AIL can be acetylated[12]; however, it remains unclear as to how many of these lysines should be acetylated to regulate equilibrium between an inhibitory (less acetylated, more positively charged) state of AIL and an activation (more acetylated, less positively charged) state of AIL. Further studies are required to establish the effect of poly-autoacetylation of AIL on this equilibrium and explore whether bromodomain is capable of targeting it, which would shift the equilibrium towards the AIL activation state facilitating the catalytic activity (Fig. 4h).

H3K18 and H3K27 acetylation requires H3-binding activity of p300-ZZ in vivo. To determine whether the H3-binding by the ZZ domain is required for p300-mediated histone acetylation in cells, we examined acetylation marks in H1299 cells stably expressing Flag-tagged wild-type or mutated p300-BRPHZT. As expected, ectopic expression of wild-type p300-BRPHZT increased the global levels of acetylation at all sites tested (Fig. 5c–f). In support of our model, p300-BRPHZT mutations that abrogate histone binding of the ZZ domain, N1671A and D1690A, or deletion of ZZ greatly attenuated the increase of H3K18 and H3K27 acetylation without affecting H3K4, H3K9, and H4 acetylation (Fig. 5c–f). Similar changes were observed in 293T cells transiently expressing full-length p300 or the ZZ-mutated counterparts (Supplementary Fig. 7b). Mutation of N1132 that disrupts acetyllysine binding of bromodo-

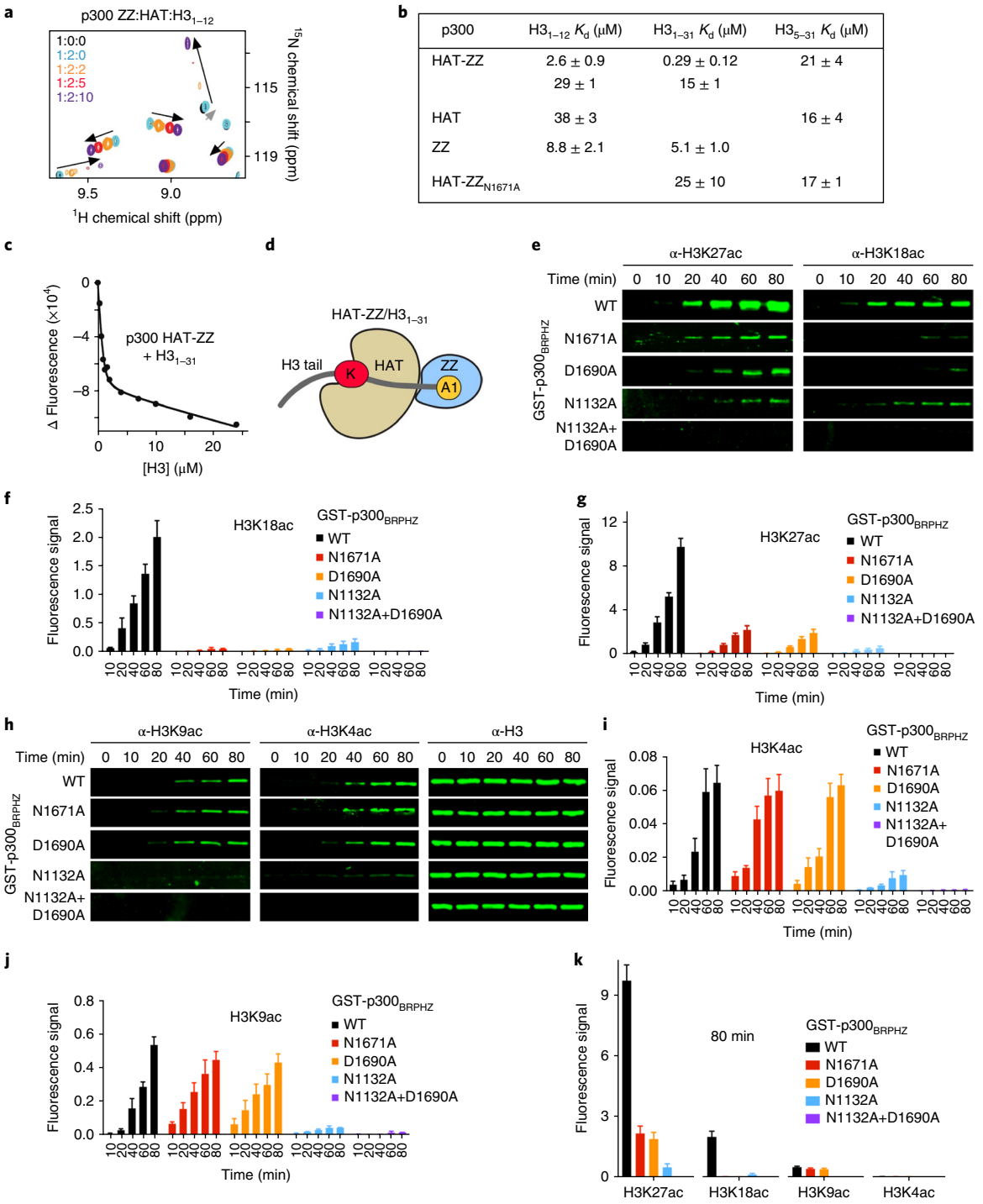

p300	H3$_{1-12}$ K_d (μM)	H3$_{1-31}$ K_d (μM)	H3$_{5-31}$ K_d (μM)
HAT-ZZ	2.6 ± 0.9 29 ± 1	0.29 ± 0.12 15 ± 1	21 ± 4
HAT	38 ± 3		16 ± 4
ZZ	8.8 ± 2.1	5.1 ± 1.0	
HAT-ZZ$_{N1671A}$		25 ± 10	17 ± 1

Fig. 3 | ZZ binding to H3 facilitates HAT activity on the distal lysine residues in H3 tail. a, Superimposed ^{1}H,^{15}N HSQC spectra of p300 ZZ collected upon titration with the unlabeled HAT domain (1:2 molar ratio) first and then with H3 peptide. Spectra are color coded according to the protein/ligands molar ratio. **b**, Binding affinities of the HAT domain, the ZZ domain, and HAT-ZZ of p300 for the indicated histone peptides as measured by tryptophan fluorescence. K_ds were calculated from triplicate measurements with the exception of H3$_{1-31}$/ZZ, which was from duplicate measurements. **c**, Representative binding curve used to determine the K_d values by fluorescence. See also Supplementary Fig. 2. **d**, Cartoon representation of HAT-ZZ in complex with H3$_{1-31}$. **e**, In vitro HAT assays using WT and mutated p300$_{BRPHZ}$ and the reconstituted nucleosome. **f**,**g**, Quantification of the HAT activity on H3K18 and H3K27 based on the fluorescence signal in **e** from three biological replicates. A common standard sample is used for normalization in each replicate. Error bars represent mean ± s.e.m. **h**, H3K9ac, H3K4ac, and H3 western blot analyses of in vitro HAT assays using wild-type and mutated p300$_{BRPHZ}$ and the reconstituted nucleosome. **i**,**j**, Quantification of the HAT activity on H3K4 and H3K9 based on the fluorescence signal from three biological replicates as in **h**. A common standard sample is used for normalization in each replicate. **k**, Comparison of the fluorescence signal for the indicated histone acetylation marks at 80 min of in vitro HAT reaction. Error bars in **f**, **g**, and **i**–**k** represent s.e.m. from three independent HAT assays using different batches of enzymes (n = 3 biological replicates). Uncropped blot images for panels **e** and **h** are shown in Supplementary Data Set 1.

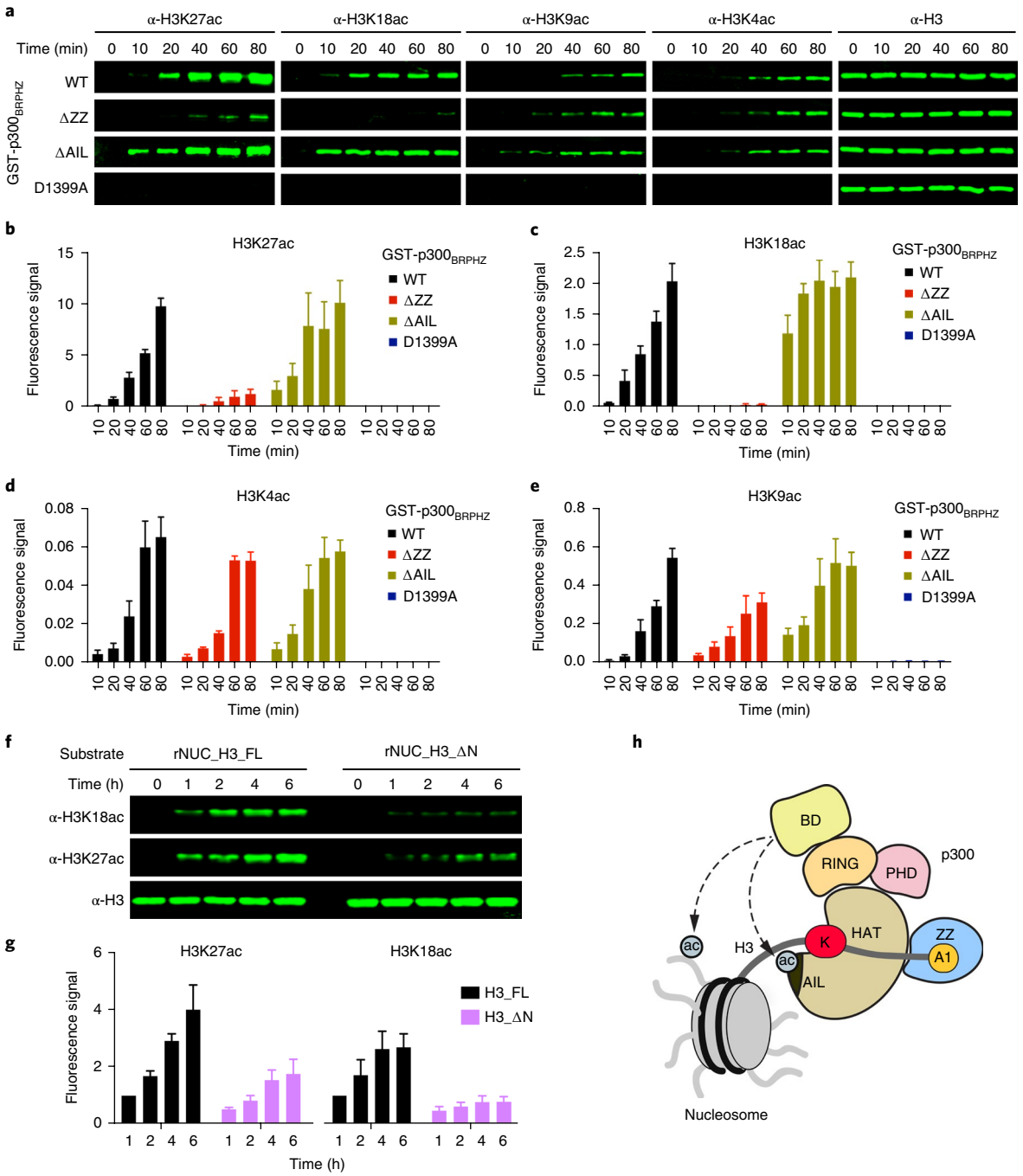

Fig. 4 | p300 ZZ-H3 interaction promotes acetylation of H3K27 and H3K18. a, In vitro HAT assays using $p300_{BRPHZ}$, wild type and counterparts harboring either ZZ deletion, AIL deletion, or loss-of-catalytic activity HAT mutation (D1399A), and the reconstituted nucleosome. **b**–**e**, Quantification of the HAT activity based on the fluorescence signal from three biological replicates. A common standard sample is used for normalization in each replicate. **f**, In vitro HAT assays using wild-type $p300_{BRPHZ}$ and the reconstituted nucleosome carrying either intact H3.1 (rNUC_H3_FL) or N-terminally truncated H3.1 (rNUC_H3_ΔN, Ala1 and Arg2 of H3.1 are deleted). **g**, Quantification of the HAT activity on H3K18 and H3K27 based on the fluorescence signal in **f** from three biological replicates. The 1-h sample of rNUC_H3_FL is used for normalization. **h**, A model for the regulation of the p300 HAT activity by the bromodomain and ZZ. Potential intermolecular interactions of bromodomain with acetylated histones and acetylated AIL are indicated by dashed lines. Error bars in **b**–**e** and **g** represent s.e.m. from three independent HAT assays using different batches of enzymes ($n = 3$ biological replicates). Uncropped blot images for panels **a** and **f** are shown in Supplementary Data Set 1.

main or deletion of bromodomain led to a reduction of acetylation at all sites; however, acetylation of H4 was most notably impeded (Fig. 5c–f). These findings indicate that while acetylation of histones, H4 in particular, by p300 requires the acetyllysine binding activity of p300-bromodomain, specific acetylation of the H3K18 and H3K27 sites[24,25] requires the H3-binding activity of p300-ZZ.

We next examined the role of the ZZ/H3 interaction in chromatin binding and acetylation function of p300-BRPHZT in H1299 cells by ChIP assays followed by high-throughput sequencing (ChIP-seq) (Fig. 6a). p300/CBP has been previously reported to associate with both H3K27 hyperacetylated active enhancers and poised regulatory regions enriched in H3K27me3[26–28]. ChIP-seq

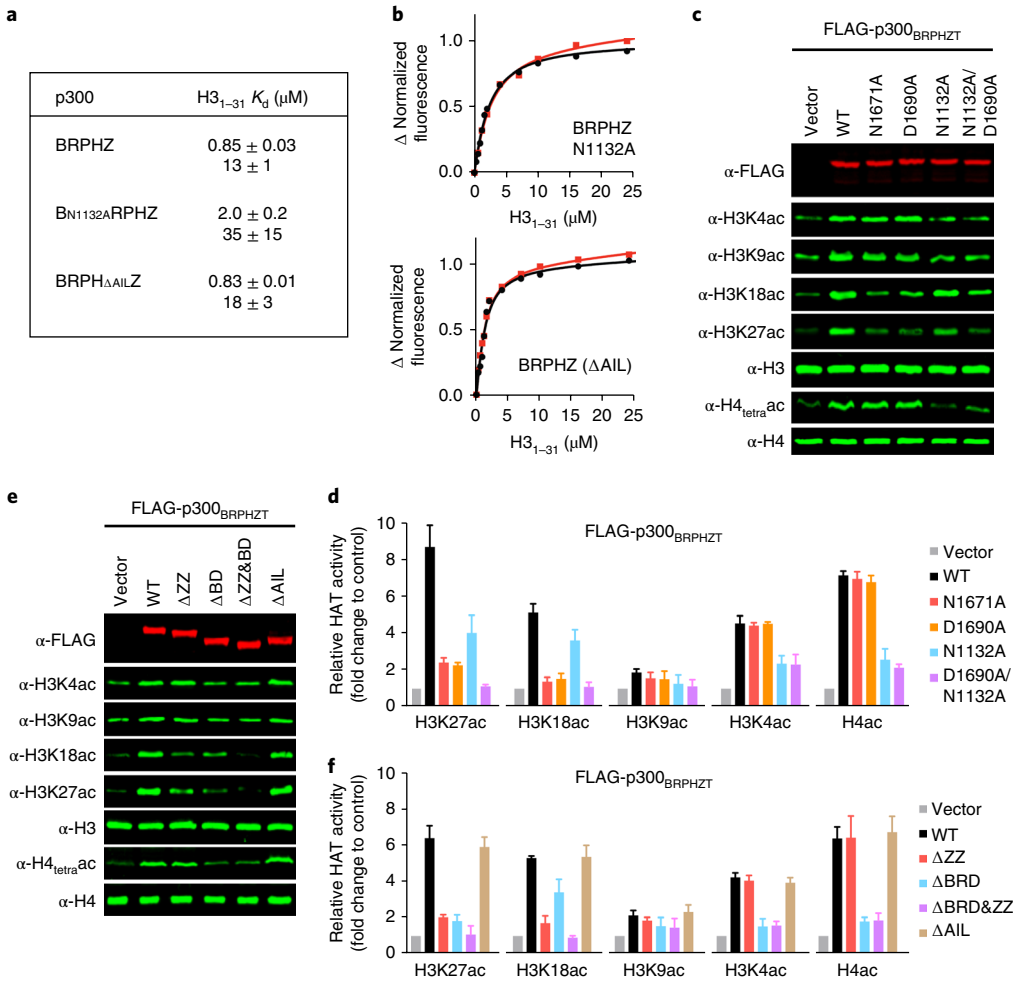

Fig. 5 | ZZ and bromodomain of p300 differentially modulate p300 activity. a, Binding affinities of p300-BRPHZ for H3$_{1-31}$ peptide measured by tryptophan fluorescence (duplicate measurements). **b**, Binding curves used to determine the K_d values by fluorescence. **c**, Western blot analysis of histone acetylation levels in whole-cell extract of H1299 cells stably expressing wild-type FLAG-p300$_{BRPHZT}$ or the indicated mutants. **d**, Quantification of the indicated histone acetylation levels from three biological replicates as in **c**. Total H3 or H4 was used for normalization. **e**, Western blot analysis of histone acetylation levels in whole-cell extract of H1299 cells stably expressing the indicated FLAG-p300$_{BRPHZT}$ fragments. **f**, Quantification of the indicated histone acetylation levels from three biological replicates as in **e**. Total H3 or H4 was used for normalization. Error bars in panels **d** and **f** represent s.e.m. from three independent batches of stable cells ($n = 3$ biological replicates). Uncropped blot images (**c** and **e**) are shown in Supplementary Data Set 1.

using the M2 Flag antibody in the cells expressing Flag-tagged wild-type p300-BRPHZT identified 679 p300-BRPHZT binding sites in both regions. An evident increase in H3K18ac and H3K27ac occupancies, especially in the regions flanking H3K27 pre-acetylated sites, was also observed in these cells (Fig. 6a,b and Supplementary Table 1). In contrast to the wild-type protein, the two ZZ domain mutants, N1671A and D1690A, were incapable of gaining the chromatin binding, and no increase in H3K18ac and H3K27ac occupancies was observed in the cells expressing these mutants (Fig. 6a,b). Furthermore, the loss-of-function mutations of the ZZ domain considerably decreased binding of p300-BRPHZT to individual genes and led to a notable reduction in the H3K18 and H3K27 acetylation levels on these genes (Fig. 6c and Supplementary Fig. 7c). Similarly, the N1132A mutation that abrogates acetyllysine binding activity of bromodomain resulted in a decrease in p300-BRPHZT occupancy and H3K18ac and H3K27ac levels at the target gene regions (Fig. 6d). Together, these results underscore the critical roles of the ZZ/H3 and bromodomain/acetyllysine interactions in p300 function in maintaining histone H3K18 and H3K27 acetylation in cells, corroborating the in vitro findings described above.

Discussion

In conclusion, we have identified a novel function for the ZZ domain of p300. It recognizes histone H3 tail through a unique and previously uncharacterized mechanism. The H3 binding activity of ZZ and the acetyllysine binding activity of bromodomain are both essential for the association of p300 with chromatin. We show that the acetyllysine binding of bromodomain is necessary for p300 to catalyze acetylation of virtually all lysine residues in H3 and H4 tested, whereas the ability of p300 to acetylate primarily H3K27 and H3K18 is due to the binding of the ZZ domain to the N terminus of H3. A model of the p300-BRPHZ/H3 complex generated using the simulated annealing method and the crystal structures of p300 BRPH[13] and H3/ZZ revealed a ~38-Å distance between the H3A1-binding site of ZZ and the catalytic site in the HAT domain (Supplementary Fig. 7d). This distance is too long for Lys9 or Lys14 of H3 to occupy the active site of the HAT domain and thus be acetylated *in cis* when the N terminus of H3 is locked through the interaction with ZZ; however, other lysine residues (K18, K23, K27) in the H3 tail can reach the active site. Furthermore, the substrate-binding groove of the HAT domain is highly negatively charged and would favor the positively charged H3 tail. Collectively, these results

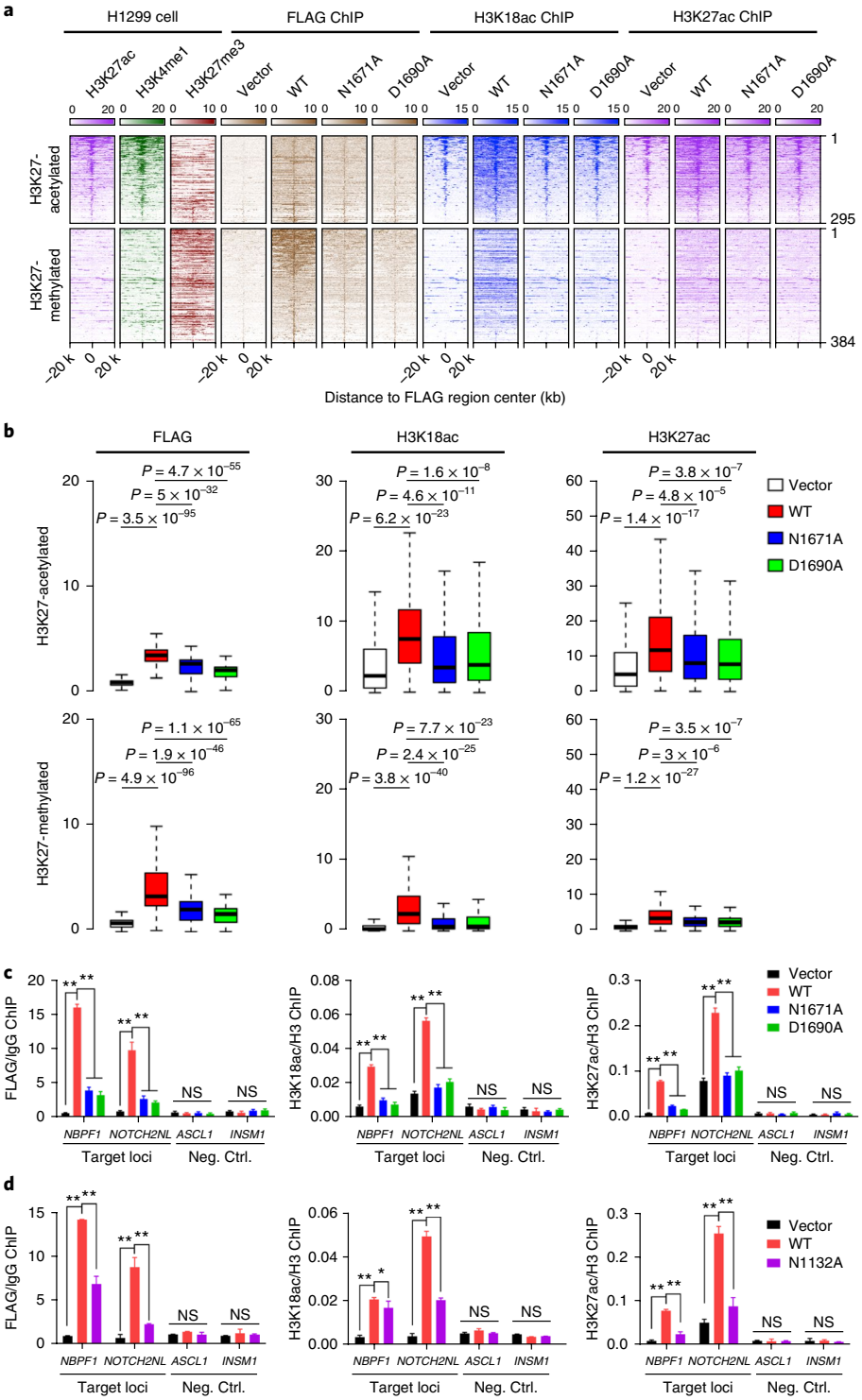

Fig. 6 | ZZ is required for binding of p300 to chromatin and its acetylation activity on H3K18 and H3K27 in cells. a, Heatmap of normalized H3K27ac (purple), H3K4me1 (green), H3K27me3 (scarlet), FLAG (brown), and H3K18ac (blue) ChIP-seq signals centered on FLAG binding sites in a ±20-kb window in H1299 control cells and H1299 cells stably expressing wild-type FLAG-p300$_{BRPHZT}$ or the indicated ZZ mutants. The color keys represent signal density. The peaks are divided into two groups (H3K27 acetylated or H3K27 methylated) based on the pre-existing H3K27 modifications at the peak center. **b**, Box plots compare FLAG, H3K18ac, and H3K27ac occupancies in different samples at FLAG binding peaks. All FLAG peaks are divided into two groups as in **a**. The center line of the box represents the median and box limits indicate the 25th and 75th percentiles. Two-tailed paired Student's *t*-test was used for statistical analyses. **c**, qPCR analysis of the FLAG-p300$_{BRPHZT}$, H3K18ac, and H3K27ac ChIP at target loci (locations indicated by black line in Supplementary Fig. 7c) and two negative control loci in H1299 cells stably expressing wild-type FLAG-p300$_{BRPHZT}$ or the indicated mutants. IgG or H3 ChIP was used for normalization. **d**, qPCR analysis of the FLAG-p300$_{BRPHZT}$, H3K18ac, and H3K27ac ChIP at target loci and two negative control loci in H1299 cells stably expressing wild-type FLAG-p300$_{BRPHZT}$ or the N1132A bromodomain mutant. IgG or H3 ChIP was used for normalization. Error bars in **c** and **d** represent s.e.m. from three individual experiments ($n = 3$ experimental repeats). $^{*}P < 0.05$; $^{**}P < 0.01$ by two-tailed unpaired *t*-test. Neg. Ctrl., negative control; NS, not significant.

suggest that binding of p300-ZZ to the N terminus of H3 provides selectivity of the HAT domain toward the distal lysine sites in H3, such as H3K18 and H3K27. Intriguingly, we found that homologous CBP-ZZ binds to H3 weakly (Supplementary Fig. 8), and it will be interesting in future studies to differentiate the biological roles of p300 and CBP that are due to different activities of their ZZ domains.

Methods

Methods, including statements of data availability and any associated accession codes and references, are available at https://doi.org/10.1038/s41594-018-0114-9.

Received: 10 May 2018; Accepted: 18 July 2018;
Published online: 27 August 2018

References

1. Wang, F., Marshall, C. B. & Ikura, M. Transcriptional/epigenetic regulator CBP/p300 in tumorigenesis: structural and functional versatility in target recognition. *Cell. Mol. Life Sci.* **70**, 3989–4008 (2013).
2. Lasko, L. M. et al. Discovery of a selective catalytic p300/CBP inhibitor that targets lineage-specific tumours. *Nature* **550**, 128–132 (2017).
3. Iyer, N. G., Ozdag, H. & Caldas, C. p300/CBP and cancer. *Oncogene* **23**, 4225–4231 (2004).
4. Dancy, B. M. & Cole, P. A. Protein lysine acetylation by p300/CBP. *Chem. Rev.* **115**, 2419–2452 (2015).
5. Goodman, R. H. & Smolik, S. CBP/p300 in cell growth, transformation, and development. *Genes Dev.* **14**, 1553–1577 (2000).
6. Bedford, D. C., Kasper, L. H., Fukuyama, T. & Brindle, P. K. Target gene context influences the transcriptional requirement for the KAT3 family of CBP and p300 histone acetyltransferases. *Epigenetics* **5**, 9–15 (2010).
7. Liu, X. et al. The structural basis of protein acetylation by the p300/CBP transcriptional coactivator. *Nature* **451**, 846–850 (2008).
8. Ogryzko, V. V., Schiltz, R. L., Russanova, V., Howard, B. H. & Nakatani, Y. The transcriptional coactivators p300 and CBP are histone acetyltransferases. *Cell* **87**, 953–959 (1996).
9. Wang, Z. et al. Genome-wide mapping of HATs and HDACs reveals distinct functions in active and inactive genes. *Cell* **138**, 1019–1031 (2009).
10. Kraus, W. L., Manning, E. T. & Kadonaga, J. T. Biochemical analysis of distinct activation functions in p300 that enhance transcription initiation with chromatin templates. *Mol. Cell. Biol.* **19**, 8123–8135 (1999).
11. Tomita, A. et al. c-Myb acetylation at the carboxyl-terminal conserved domain by transcriptional co-activator p300. *Oncogene* **19**, 444–451 (2000).
12. Thompson, P. R. et al. Regulation of the p300 HAT domain via a novel activation loop. *Nat. Struct. Mol. Biol.* **11**, 308–315 (2004).
13. Delvecchio, M., Gaucher, J., Aguilar-Gurrieri, C., Ortega, E. & Panne, D. Structure of the p300 catalytic core and implications for chromatin targeting and HAT regulation. *Nat. Struct. Mol. Biol.* **20**, 1040–1046 (2013).
14. Andrews, F. H., Strahl, B. D. & Kutateladze, T. G. Insights into newly discovered marks and readers of epigenetic information. *Nat. Chem. Biol.* **12**, 662–668 (2016).
15. Musselman, C. A., Lalonde, M. E., Cote, J. & Kutateladze, T. G. Perceiving the epigenetic landscape through histone readers. *Nat. Struct. Mol. Biol.* **19**, 1218–1227 (2012).
16. Taverna, S. D., Li, H., Ruthenburg, A. J., Allis, C. D. & Patel, D. J. How chromatin-binding modules interpret histone modifications: lessons from professional pocket pickers. *Nat. Struct. Mol. Biol.* **14**, 1025–1040 (2007).
17. Filippakopoulos, P. et al. Histone recognition and large-scale structural analysis of the human bromodomain family. *Cell* **149**, 214–231 (2012).
18. Ragvin, A. et al. Nucleosome binding by the bromodomain and PHD finger of the transcriptional cofactor p300. *J. Mol. Biol.* **337**, 773–788 (2004).
19. Park, S. et al. Role of the CBP catalytic core in intramolecular SUMOylation and control of histone H3 acetylation. *Proc. Natl Acad. Sci. USA* **114**, E5335–E5342 (2017).
20. Park, S., Martinez-Yamout, M. A., Dyson, H. J. & Wright, P. E. The CH2 domain of CBP/p300 is a novel zinc finger. *FEBS Lett.* **587**, 2506–2511 (2013).
21. Plotnikov, A. N. et al. Structural insights into acetylated-histone H4 recognition by the bromodomain-PHD finger module of human transcriptional coactivator CBP. *Structure* **22**, 353–360 (2014).
22. Mujtaba, S. et al. Structural mechanism of the bromodomain of the coactivator CBP in p53 transcriptional activation. *Mol. Cell* **13**, 251–263 (2004).
23. Das, C. et al. Binding of the histone chaperone ASF1 to the CBP bromodomain promotes histone acetylation. *Proc. Natl Acad. Sci. USA* **111**, E1072–E1081 (2014).
24. Jin, Q. et al. Distinct roles of GCN5/PCAF-mediated H3K9ac and CBP/p300-mediated H3K18/27ac in nuclear receptor transactivation. *EMBO J.* **30**, 249–262 (2011).
25. Tang, Z. et al. SET1 and p300 act synergistically, through coupled histone modifications, in transcriptional activation by p53. *Cell* **154**, 297–310 (2013).
26. Rada-Iglesias, A. et al. A unique chromatin signature uncovers early developmental enhancers in humans. *Nature* **470**, 279–283 (2011).
27. Buecker, C. & Wysocka, J. Enhancers as information integration hubs in development: lessons from genomics. *Trends Genet.* **28**, 276–284 (2012).
28. Zentner, G. E., Tesar, P. J. & Scacheri, P. C. Epigenetic signatures distinguish multiple classes of enhancers with distinct cellular functions. *Genome Res.* **21**, 1273–1283 (2011).

Acknowledgements

We thank J. Nix at beam line 4.2.2 of the ALS in Berkeley for help with X-ray crystallographic data collection. This work was supported by grants from NIH GM106416, GM125195, and GM100907 to T.G.K., CA204020 to X.S., and HG007538 and CA193466 to W.L., and from the Cancer Prevention and Research Institute of Texas (RP160237 and RP160739), the Welch Foundation (G1719), and the Leukemia & Lymphoma Society Career Development Program Scholarship to X.S.

Author contributions

Y.Z., Y.X., J.S., J.W.A., W.M., M.A., X.W., B.J.K., and H.W. performed experiments and together with W.L., X.S., and T.G.K. analyzed the data. Y.Z., X.S., and T.G.K. wrote the manuscript with input from all authors.

Competing interests

The authors declare no competing interests.

Additional information

Supplementary information is available for this paper at https://doi.org/10.1038/s41594-018-0114-9.

Reprints and permissions information is available at www.nature.com/reprints.

Correspondence and requests for materials should be addressed to X.S. or T.G.K.

Publisher's note: Springer Nature remains neutral with regard to jurisdictional claims in published maps and institutional affiliations.

Methods

Materials. The coding DNA sequences encoding human full-length p300 protein and the p300 BRPHZT region (amino acids 1,035–1,830) were cloned into pENTR3C vector and subsequently cloned into p3FLAG and pCDH-FLAG destination vectors using Gateway techniques (Invitrogen), respectively. The coding DNA sequences encoding the human p300 bromodomain-RING-PHD-HAT-ZZ region (BRPHZ, amino acids 1,035–1,720) and ZZ domain (amino acids 1,650–1,720) were cloned into the pGEX-6P-1 vector (GE Healthcare). Point mutations and deletions were generated using a site-directed mutagenesis kit (Stratagene) and verified by Sanger sequencing. Histone peptides bearing different modifications were synthesized at CPC, LLC. Anti-histone antibodies including anti-H3 (Ab1791), anti-H3K4ac (ab176799), anti-H3K9ac (Ab32129), anti-H3K27ac (Ab4729), and anti-H4 (Ab7311) were obtained from Abcam. Anti-H3K9ac (61251) and anti-H3K18ac (39755) antibodies were from Active Motif. Anti-acetyl-Histone H4 antibody (06-598) was from Millipore. Anti-GST (sc-459) antibody was from Santa Cruz. Anti-FLAG (M2, F1804) antibody was from Sigma. Fluorescent secondary antibodies (926-32211 and 926-68020) were from LI-COR. Mononucleosomes reconstituted from recombinant histones (16-0009) were from EpiCypher.

Protein expression and purification for pull-down assays. p300-BRPHZ and p300-ZZ cloned in the pGEX-6P-1 vector were expressed in BL21 Rosetta 2 cells. Protein production was induced with 0.2 mM isopropyl-β-D-thiogalactoside and cultured overnight at 16 °C in Luria broth medium supplemented with 0.05 mM $ZnCl_2$. The GST-tagged proteins were purified on glutathione Sepharose 4B beads (Amersham) in binding buffer (50 mM Tris-HCl pH 7.5, 150 mM NaCl, 0.05% NP-40, 1 mM phenylmethyl sulfonyl fluoride, plus protease inhibitors (Roche)) and eluted by 100 mM Tris pH 8.0 containing 15 mg ml^{-1} reduced glutathione (Sigma). All proteins harboring mutations or deletions were expressed and purified as wild-type proteins.

Peptide pull-down assays. Peptide pull-down assays were performed as described previously[29]. In brief, 1 µg biotinylated histone peptides with different modifications were incubated with 1–2 µg GST-fused p300 ZZ domain in binding buffer (50 mM Tris-HCl pH 7.5, 300 mM NaCl, 0.1% NP-40, 1 mM phenylmethyl sulfonyl fluoride) overnight with rotation at 4 °C. Streptavidin beads (Amersham) were added to the mixture, and the mixture was incubated for 1 h with rotation at 4 °C. The beads were then washed three times and the bound proteins were analyzed using SDS–PAGE and western blotting.

Calf thymus histone pull-down assay. Full-length histone pull-down assays were performed as described previously[30]. Briefly, 2 µg GST-tagged protein was incubated with 10 µg calf thymus total histones (Worthington) in binding buffer (50 mM Tris-HCl pH 7.5, 1 M NaCl, 1% NP-40) at 4 °C overnight with rotation. Glutathione Sepharose 4B beads (Amersham) were added to the solution and incubated for 1 h. The beads were then washed six times and bound histones were detected using SDS–PAGE and western blotting.

Salt fractionation. Salt fractionation of nuclei was performed as previously described[31]. In short, cells were swollen with hypotonic buffer (10 mM HEPES pH 7.9, 1.5 mM $MgCl_2$, 10 mM KCl) and lysed by gentle disruption to isolate nuclei. The nuclei were incubated with wash buffer (20 mM HEPES pH 7.9, 1.5 mM $MgCl_2$, 0.2 mM EDTA, 25% glycerol) containing 75 mM NaCl for 30 min at 4 °C and then pelleted and the supernatant fraction was collected. The nuclei were then similarly washed by wash buffer containing 150 mM, 300 mM, and 600 mM NaCl and the supernatant fraction of each step was collected. After the final wash step, the pellet was resuspended and sonicated before collection.

Protein expression and purification for structural studies. The human p300 ZZ domain (amino acids 1,663–1,713) and H3-linked ZZ domain (H3 amino acids 1–6, ZZ amino acids 1,663–1,713) were cloned into a pCIOX vector with N-terminal His-tag and Ulp1 cleavage site. The p300 HAT domain (amino acids 1,287–1,663, Y1467F), HAT-ZZ domain (amino acids 1,287–1,713, Y1467F), and BRP region (amino acids 1,047–1,278) were cloned into a pDEST-17 vector with N-terminal His-tag and PreScission cleavage site. The p300 $ZZ_{1,668}$ domain (amino acids 1,668–1,713) and CBP ZZ (amino acids 1,705–1,750) were cloned into a pCOOL vector with N-terminal GST tag and Thrombin cleavage site. All proteins were expressed in BL21 (DE3) RIL cells. Protein production was induced with 0.2 mM isopropyl-β-D-thiogalactoside and incubated overnight at 18 °C in Luria broth or minimal media (M9) supplemented with $^{15}NH_4Cl$ and 0.05 mM $ZnCl_2$. The His-tag proteins were purified on Ni-NTA beads (Qiagen) in 20 mM Tris-HCl (pH 7.5) buffer, supplemented with 300 mM NaCl and 10 mM ßME. The His-tag was cleaved overnight at 4 °C with PreScission or Ulp1 protease. The GST-tagged proteins were purified on glutathione Sepharose 4B beads (GE Healthcare) in 20 mM Tris-HCl (pH 7.0) buffer, supplemented with 100 mM NaCl and 5 mM dithiothreitol. The GST tag was cleaved overnight at 4 °C with Thrombin protease. The GST-tagged p300-BRPHZ and mutants were purified as above and cleaved overnight at 4 °C with PreScission. Unlabeled proteins were further purified by size exclusion chromatography and concentrated in Millipore concentrators.

All mutants were generated by site-directed mutagenesis using the Stratagene QuickChange mutagenesis protocol, and grown and purified as wild-type proteins.

NMR experiments. NMR experiments were carried out at 298 K on Varian INOVA 600 MHz and 900 MHz spectrometers. NMR samples contained 0.1 mM uniformly ^{15}N-labeled wild-type or mutated p300-ZZ, p300-HAT-ZZ, p300-bromodomain-RING-PHD, and CBP-ZZ proteins in 20 mM Tris-HCl (pH 7.0) buffer supplemented with 100 mM NaCl, 5 mM dithiothreitol, and 8% D_2O. Binding was characterized by monitoring chemical shift changes in the proteins induced by histone peptides (synthesized by SynPeptide).

X-ray crystallography. The p300 H3-linked ZZ domain (amino acids 1,663–1,713) was crystallized. For crystallization, the purified H3–ZZ (15 mg ml^{-1}) was buffer exchanged into 5 mM HEPES (pH 7.4), 50 mM NaCl, and 0.5 mM TCEP before crystallization. Good quality diffracting crystals were obtained at 4 °C in 0.1 M HEPES and 70% MPD (pH 7.5). Data collection was performed at the ALS 4.2.2 beamline, Berkeley. HKL3000 was used for indexing, scaling, and data reduction. Solution was found by the single-wavelength anomalous dispersion method with Zn anomalous signal. Manual model building was performed using Coot[32] and the structure was refined using Phoenix Refine[33]. The final structure was verified by MOLProbity[34] showing 94.1% and 5.9% of residues in the most favored regions and additionally allowed regions, respectively. The X-ray diffraction and structure refinement statistics are summarized in Table 1.

Fluorescence spectroscopy. Spectra were recorded at 25 °C on a Fluoromax-3 spectrofluorometer (HORIBA) as described previously[35] with the following modifications. The samples containing 1.0 µM p300 ZZ, HAT, HAT-ZZ, and HAT-ZZ_{N1671A} with Y1467F mutation, BRPHZ, B_{N1132A}RPHZ, or $BRPH_{\Delta AIL}Z$ and progressively increasing concentrations of the histone peptide were excited at 295 nm. All experiments were performed in buffer containing 15 mM HEPES (pH 7.2), 150 mM NaCl, and 0.5 mM TCEP. Emission spectra were recorded over a range of wavelengths between 330 nm and 360 nm with a 0.5-nm step size and a 1-s integration time and averaged over three scans. The K_d values were determined using a non-linear least-squares analysis in Kaleidagraph and the equation:

$$\Delta I = \Delta I_{max} \frac{(([L] + [P] + K_d) - \sqrt{([L] + [P] + K_d)^2 - (4[P][L])})}{2[P]}$$

where $[L]$ is the concentration of the histone peptide, $[P]$ is the protein concentration, ΔI is the observed change of signal intensity, and ΔI_{max} is the difference in signal intensity of the free and bound states. Binding curves of HAT-ZZ, BRPHZ, B_{N1132A}RPHZ, or $BRPH_{\Delta AIL}Z$ were fit by a non-linear least-squares analysis in Kaleidagraph using a two-site binding model:

$$\Delta I = \Delta I_{max,1} \left\{ \frac{(([L] + [P] + K_{d1}) - \sqrt{([L] + [P] + K_{d1})^2 - (4[P][L])})}{2[P]} + \left(\Delta I_{max,2} \frac{[L]}{K_{d2}} + [L] \right) \right\}$$

The K_d values were averaged over three or two separate experiments as stated in corresponding figure legends, with error calculated as the standard deviation between the runs.

Modeling of the H3-bound BRPHZ region of p300. The model of the complex of p300 BRDHZ (amino acids 1,047–1,713) with H3 tail (1–31) was generated using the crystal structure of BRDH (Protein Data Bank (PDB) 4BHW)[13] and the H3–ZZ complex and the simulated annealing method in Xplor-NIH[36]. The lysine portion of the bi-substrate Lys-CoA was modified into the side chain of Lys27 of H3, and then the H3/ZZ complex was modeled onto the crystal structure with a flexible linker (residues 1,661–1,664). The model of the complex was treated as an initial structure and refined by simulated annealing. During the refinement, the backbone atoms of BRDH region (amino acids 1,047–1,660) were fixed, whereas the backbone atoms of the H3(amino acids 1–4)/ZZ(amino acids 1,665–1,713) complex were grouped and allowed to move as a rigid body. Distances between the Lys-CoA and residues W1436 and S1396 in the crystal structure were used as additional restraints to maintain the active site conformation. At all times, residues 1,661–1,664 of p300 and residues 5–31 of H3 were set to be fully flexible. Twenty models were calculated and six structures with the lowest energy were selected for further analysis.

In vitro HAT assays. For HAT assays on recombinant nucleosomes containing full-length histone H3.1, purified wild-type or mutated $p300_{BRPHZ}$ (300 nM) was incubated with recombinant mononucleosome (100 nM) in HAT reaction buffer (50 mM Tris pH 8.0, 0.1 mM EDTA, 10% glycerol, 1 mM phenylmethyl sulfonyl fluoride, and 1 mM dithiothreitol) in a total volume of 50 µl. After prewarming at 37 °C for 5 min, reactions were initiated with the addition of acetyl-CoA (Sigma) to

a final concentration of 0.1 mM and incubated for 10~80 min at 37 °C. For assays comparing the HAT activities on recombinant nucleosomes containing full-length histone H3.1 and N-terminally truncated H3.1, wild-type $p300_{BRPHZ}$ fragment (50 nM) and mononucleosome (500 nM) were incubated under the same condition for 1–6 h. Reactions were quenched by flash-freezing in liquid nitrogen and then analyzed by SDS–PAGE and western blot analysis. Western blot results were quantified by LI-COR Odyssey and normalized to a common standard sample.

Cell culture, transfection, and virus transduction. HEK293T cell (ATCC) was maintained in DMEM (Cellgro) supplemented with 10% fetal bovine serum (Sigma). Human lung cancer cell line H1299 (ATCC) was maintained in RPMI (Cellgro) supplemented with 10% fetal bovine serum (Sigma). Both cell lines were mycoplasma-negative and were tested for authentication by short tandem repeat profiling performed by the MDACC CCSG-funded Characterized Cell Line Core, NCI CA016672. Transient transfection was performed using X-tremeGENE DNA transfection reagent (Sigma). At 48 h after transfection, cells were collected for western blot analysis. Lentiviral transduction was performed as described previously[37]. Briefly, 293T cells were cotransfected with pMD2.G, pPAX2 (Addgene), and pCDH cDNA constructs using X-tremeGENE DNA transfection reagent (Roche). For infections, H1299 cells were incubated with viral supernatants in the presence of 8 mg ml^{-1} polybrene; after 48 hr, the infected cells were selected with blasticidin (10 mg ml^{-1}) for 4–6 d before experiments.

ChIP and ChIP-seq. ChIP analysis was performed essentially as described previously[37,38]. In brief, cells were cross-linked with 1% formaldehyde for 10 min and stopped with 125 mM glycine. The isolated nuclei were resuspended in nuclei lysis buffer (50 mM Tris pH 8.0, 10 mM EDTA, 1% SDS) and sonicated using a Bioruptor Sonicator (Diagenode). The samples were immunoprecipitated with 2–4 µg of the appropriate antibodies overnight at 4 °C. Protein A/G beads (Millipore) were added and incubated for 1 h, and the immunoprecipitates were washed twice, each with low-salt (20 mM Tris pH 8.0, 150 mM NaCl, 2 mM EDTA, 1% Triton X-100, and 0.1% SDS), high-salt (20 mM Tris pH 8.0, 500 mM NaCl, 2 mM EDTA, 1% Triton X-100, and 0.1% SDS), and LiCl buffers (20 mM Tris pH 8.0, 250 mM LiCl, 1 mM EDTA, 1% NP-40, and 1% SDS). Eluted DNA was reverse-cross-linked, purified using PCR purification kit (Qiagen), and analyzed by quantitative real-time PCR on the ABI 7500-FAST System using the Power SYBR Green PCR Master Mix (Applied Biosystems).

For ChIP-seq, the ChIP experiments were carried out essentially as described above. Purified DNA was sequenced using the Illumina Solexa Hiseq 3000. The raw reads were mapped to human reference genome NCBI 37 (hg19) or the *Drosophila melanogaster* genome (dm3) by bowtie v1.1.0, allowing up to one mismatch. Only uniquely mapped reads were retained for peak calling. But, before that, we used spike-in normalization for sample size correction as previously described[39]. For simplicity, the reads were downsampled to keep the same spike-in reads count in different samples. Then, the ChIP-seq peaks were called by MACS v1.4.2 with a cut-off of $P \leq 1\times10^{-8}$, and clonal reads were automatically removed by MACS. The ChIP-seq reads density was determined by deepTools v2.3.4, and then the average binding profile and heatmap were visualized using R v3.2.3 (Supplementary Tables 1–4).

Protein-ChIP. Protein-ChIP assays for detection of in situ p300–chromatin interactions were performed as described previously[40]. Briefly, cells were cross-linked with 1% formaldehyde for 10 min and stopped with 125 mM glycine. The isolated nuclei were resuspended in nuclei lysis buffer and sonicated. Anti-FLAG M2-conjugated agarose beads (Sigma) were incubated with lysates overnight at 4 °C. The beads were then washed twice, each with low-salt, high-salt, and LiCl buffers, and the bound proteins were analyzed by SDS–PAGE and western blot.

Statistical analyses. Experimental data are presented as mean ± s.e.m. unless stated otherwise. Statistical significance was calculated by two-tailed unpaired *t*-test on two experimental conditions with $P < 0.05$ considered statistically significant unless stated otherwise. Statistical significance levels are denoted as follows: $^{*}P < 0.05$; $^{**}P < 0.01$. No statistical methods were used to predetermine sample size.

Reporting summary. Further information on experimental design is available in the Nature Research Reporting Summary linked to this article.

Data availability. The atomic coordinates and structure factors of p300 ZZ/H3 have been deposited in PDB under accession code 6DS6. The ChIP-seq data have been submitted to the Gene Expression Omnibus under accession GSE109591. Other data are available from the corresponding authors on reasonable request.

References

29. Klein, B. J. et al. PHF20 readers link methylation of histone H3K4 and p53 with H4K16 acetylation. *Cell Rep.* **17**, 1158–1170 (2016).
30. Wen, H. et al. ZMYND11 links histone H3.3K36me3 to transcription elongation and tumour suppression. *Nature* **508**, 263–268 (2014).
31. Teves, S. S. et al. A dynamic mode of mitotic bookmarking by transcription factors. *eLife* **5**, (2016).
32. Emsley, P., Lohkamp, B., Scott, W. G. & Cowtan, K. Features and development of Coot. *Acta Crystallogr. D Biol. Crystallogr.* **66**, 486–501 (2010).
33. Adams, P. D. et al. PHENIX: a comprehensive Python-based system for macromolecular structure solution. *Acta Crystallogr. D Biol. Crystallogr.* **66**, 213–221 (2010).
34. Chen, V. B. et al. MolProbity: all-atom structure validation for macromolecular crystallography. *Acta Crystallogr. D Biol. Crystallogr.* **66**, 12–21 (2010).
35. Gatchalian, J. et al. Dido3 PHD modulates cell differentiation and division. *Cell Rep.* **4**, 148–158 (2013).
36. Schwieters, C. D., Kuszewski, J. J., Tjandra, N. & Clore, G. M. The Xplor-NIH NMR molecular structure determination package. *J. Magn. Reson.* **160**, 65–73 (2003).
37. Li, Y. et al. AF9 YEATS domain links histone acetylation to DOT1L-mediated H3K79 methylation. *Cell* **159**, 558–571 (2014).
38. Wan, L. et al. ENL links histone acetylation to oncogenic gene expression in acute myeloid leukaemia. *Nature* **543**, 265–269 (2017).
39. Egan, B. et al. An alternative approach to ChIP-seq normalization enables detection of genome-wide changes in histone H3 lysine 27 trimethylation upon EZH2 inhibition. *PloS One* **11**, e0166438 (2016).
40. Ricke, R. M. & Bielinsky, A. K. Easy detection of chromatin binding proteins by the Histone Association Assay. *Biol. Proced. Online* **7**, 60–69 (2005).

nature research

Corresponding author(s): Kutateladze

Reporting Summary

Nature Research wishes to improve the reproducibility of the work that we publish. This form provides structure for consistency and transparency in reporting. For further information on Nature Research policies, see Authors & Referees and the Editorial Policy Checklist.

Statistical parameters

When statistical analyses are reported, confirm that the following items are present in the relevant location (e.g. figure legend, table legend, main text, or Methods section).

n/a	Confirmed	
☐	☒	The exact sample size (*n*) for each experimental group/condition, given as a discrete number and unit of measurement
☐	☒	An indication of whether measurements were taken from distinct samples or whether the same sample was measured repeatedly
☐	☒	The statistical test(s) used AND whether they are one- or two-sided *Only common tests should be described solely by name; describe more complex techniques in the Methods section.*
☒	☐	A description of all covariates tested
☒	☐	A description of any assumptions or corrections, such as tests of normality and adjustment for multiple comparisons
☐	☒	A full description of the statistics including central tendency (e.g. means) or other basic estimates (e.g. regression coefficient) AND variation (e.g. standard deviation) or associated estimates of uncertainty (e.g. confidence intervals)
☐	☒	For null hypothesis testing, the test statistic (e.g. *F*, *t*, *r*) with confidence intervals, effect sizes, degrees of freedom and *P* value noted *Give P values as exact values whenever suitable.*
☒	☐	For Bayesian analysis, information on the choice of priors and Markov chain Monte Carlo settings
☒	☐	For hierarchical and complex designs, identification of the appropriate level for tests and full reporting of outcomes
☒	☐	Estimates of effect sizes (e.g. Cohen's *d*, Pearson's *r*), indicating how they were calculated
☐	☒	Clearly defined error bars *State explicitly what error bars represent (e.g. SD, SE, CI)*

Our web collection on statistics for biologists may be useful.

Software and code

Policy information about availability of computer code

Data collection	X-ray crystallographic data were collected at beam line 4.2.2 of the ALS in Berkeley
Data analysis	PHENIX, Coot, PyMOL and other software listed in the Method section. Software for ChIP-seq analysis include bowtie v1.1.0; MACS v1.4.2; deepTools v2.3.4; R v3.2.3.

For manuscripts utilizing custom algorithms or software that are central to the research but not yet described in published literature, software must be made available to editors/reviewers upon request. We strongly encourage code deposition in a community repository (e.g. GitHub). See the Nature Research guidelines for submitting code & software for further information.

Data

Policy information about availability of data

All manuscripts must include a data availability statement. This statement should provide the following information, where applicable:

- Accession codes, unique identifiers, or web links for publicly available datasets
- A list of figures that have associated raw data
- A description of any restrictions on data availability

Coordinates and structure factors have been deposited in the Protein Data Bank under the accession code 6DS6. The ChIP-seq data is submitted to Gene Expression Omnibus under the accession number GSE109591. Other data are available from the corresponding authors upon reasonable request.

Field-specific reporting

Please select the best fit for your research. If you are not sure, read the appropriate sections before making your selection.

☒ Life sciences ☐ Behavioural & social sciences ☐ Ecological, evolutionary & environmental sciences

For a reference copy of the document with all sections, see nature.com/authors/policies/ReportingSummary-flat.pdf

Life sciences study design

All studies must disclose on these points even when the disclosure is negative.

Sample size	present in relevant figure legends
Data exclusions	no data exclusions
Replication	present in relevant figure legends
Randomization	no randomization
Blinding	no blinding

Reporting for specific materials, systems and methods

Materials & experimental systems

n/a	Involved in the study
☒	☐ Unique biological materials
☐	☒ Antibodies
☐	☒ Eukaryotic cell lines
☒	☐ Palaeontology
☒	☐ Animals and other organisms
☒	☐ Human research participants

Methods

n/a	Involved in the study
☐	☒ ChIP-seq
☒	☐ Flow cytometry
☒	☐ MRI-based neuroimaging

Antibodies

Antibodies used	Antibodies used for ChIP are described in the ChIP-seq report section. Antibodies used for other assays: Anti-histone antibodies including anti-H3 (Ab1791), anti-H3K4ac (ab176799), anti-H3K9ac (Ab32129), anti-H3K27ac (Ab4729) and anti-H4 (Ab7311) antibodies were obtained from Abcam. Anti-H3K9ac (61251) and anti-H3K18ac (39755) antibodies were from Active Motif. Anti-acetyl-Histone H4 antibody (06-598) was from Millipore. Anti-GST (sc-459) antibody was from Santa Cruz. Anti-FLAG (M2, F1804) antibody was from Sigma. Fluorescent secondary antibodies (926-32211 and 926-68020) were from LI-COR.
Validation	All antibodies validation are available on the manufacturers' websites.

Eukaryotic cell lines

Policy information about cell lines

Cell line source(s)	Human cell lines HEK293T and H1299 are from ATCC.
Authentication	Both cell lines were tested for authentication by short tandem repeat (STR) profiling performed by the MDACC CCSG-funded Characterized Cell Line Core, NCI CA016672.
Mycoplasma contamination	Both cell lines were tested negative for mycoplasma contamination by PCR analysis.
Commonly misidentified lines (See ICLAC register)	N/A

ChIP-seq

Data deposition

☒ Confirm that both raw and final processed data have been deposited in a public database such as GEO.

☒ Confirm that you have deposited or provided access to graph files (e.g. BED files) for the called peaks.

Data access links *May remain private before publication.*	https://www.ncbi.nlm.nih.gov/geo/query/acc.cgi?acc=GSE109591 Secure token: mtepqgcinvehhcl
Files in database submission	1671_FLAG.bw 1671_H3K18ac.bw 1671_H3K27ac.bw 1690_FLAG.bw 1690_H3K18ac.bw 1690_H3K27ac.bw V_FLAG.bw V_H3K18ac.bw V_H3K27ac.bw WT_FLAG.bw WT_H3K18ac.bw WT_H3K27ac.bw WT_Input.bw
Genome browser session (e.g. UCSC)	no longer applicable

Methodology

Replicates	FLAG ChIP in Vector, WT, N1671A and D1690A: 1 replicate H3K18ac ChIP in Vector, WT, N1671A and D1690A: 1 replicate H3K27ac ChIP in Vector, WT, N1671A and D1690A: 1 replicate
Sequencing depth	Samples Total.Reads Mapped.Reads Mapping.Ratio 1671_FLAG 70,234,624 54,491,675 77.59% 1690_FLAG 66,586,760 50,273,983 75.50% V_FLAG 54,136,479 37,054,551 68.45% WT_FLAG 65,279,501 51,230,399 78.48% 1671_H3K18ac 60,662,571 52,370,179 86.33% 1690_H3K18ac 73,047,304 63,761,261 87.29% V_H3K18ac 64,687,819 55,772,827 86.22% WT_H3K18ac 57,224,732 49,694,971 86.84% 1671_H3K27ac 85,080,095 73,888,843 86.85% 1690_H3K27ac 47,932,277 41,639,992 86.87% V_H3K27ac 65,122,868 56,715,609 87.09% WT_H3K27ac 70,235,027 60,873,057 86.67% WT_Input 71,482,836 58,990,271 82.52% Note: Reads in all samples are single-end and in 50bp length.
Antibodies	FLAG antibody: Sigma F1804. H3K18ac antibody: Active Motif 39755. H3K27ac antibody: Abcam Ab4729.
Peak calling parameters	macs14 -t alignmentA.bed -n sampleA --nomodel --nolambda -g hs --wig -S -p 1e-8
Data quality	P < 1e-8 was used as cutoff to identify peaks. sample peak_count WT_FLAG 568 WT_H3K18ac 41198 WT_H3K27ac 41451 1671_FLAG 514 1671_H3K18ac 29603 1671_H3K27ac 28120 1690_FLAG 457 1690_H3K18ac 29952 1690_H3K27ac 30129
Software	bowtie v1.1.0; MACS v1.4.2; deepTools v2.3.4; R v3.2.3.